# Distinct mechanoreceptor *pezo-1* isoforms modulate food intake in the nematode *Caenorhabditis elegans*

Hughes K[1§], Shah A[1§], Bai X[2], Adams J[1], Bauer R[2,4], Jackson J[1], Bainbridge C[1], Harris E[1], Ficca A[1], Freebairn P[1], Mohammed S[1], Fernández EM[3], Brocco MA[3], Stein W[1], Vidal-Gadea AG[1*]

[1]School of Biological Sciences, Illinois State University, Normal, IL, USA
[2]National Institute of Diabetes and Digestive and Kidney Diseases, National Institutes of Health, Bethesda, MD, USA
[3]Instituto de Investigaciones Biotecnológicas, Universidad Nacional de San Martín (UNSAM); Consejo Nacional de Investigaciones Científicas y Técnicas (CONICET) San Martín; Buenos Aires, Argentina
[4]Current Address: Feinberg School of Medicine, Northwestern University, IL, USA
[§]Contributed equally to this manuscript
*avidal@ilstu.edu

**Abstract:**
Two PIEZO mechanosensitive cation channels, PIEZO1 and PIEZO2, have been identified in mammals, where they are involved in numerous sensory processes. While structurally similar, PIEZO channels are expressed in distinct tissues and exhibit unique properties. How different PIEZOs transduce force, how their transduction mechanism varies, and how their unique properties match the functional needs of the distinct tissues where they are expressed remain all-important unanswered questions. The nematode *Caenorhabditis elegans* has a single PIEZO ortholog (*pezo-1*) predicted to have twelve isoforms. These isoforms share many transmembrane domains, but differ in those that distinguish PIEZO1 and PIEZO2 in mammals. Here we use translational and transcriptional reporters to show that long *pezo-1* isoforms are selectively expressed in mesodermally derived tissues (such as muscle and glands). In contrast, shorter *pezo-1* isoforms are primarily expressed in neurons. In the digestive system, different *pezo-1* isoforms appear to be expressed in different cells of the same organ. We show that pharyngeal muscles, glands, and valve rely on long *pezo-1* isoforms to respond appropriately to the presence of food. The unique pattern of complementary expression of *pezo-1* isoforms suggest that different isoforms possess distinct functions. The number of *pezo-1* isoforms in *C. elegans*, their differential pattern of expression, and their roles in experimentally tractable processes make this an attractive system to investigate the molecular basis for functional differences between members of the PIEZO family of mechanoreceptors.

**Introduction:**
The ability to accurately sense and respond to mechanical forces is of utmost importance for a wide range of biological processes important for survival. Mechanoreceptor proteins are instrumental in sensing mechanical forces, and they are the most versatile class of sensory transductors. They have been implicated not just in touch, but also in many sensory modalities including hearing, balance, osmosensation, hygrosensation, pain sensation, and more (Liu et al., 2007; Murthy et al., 2018; Rosenbaum et al., 2020). Reflecting this diversity of roles, mechanoreceptors play crucial roles in many processes ranging from gating predator-prey interaction (e.g. crayfish tail flip, or fish C-start escape) (Currie, 1991; Katoh et al., 2013) to monitor limb position (Woo et al., 2015a) and internal organ pressure (e.g. crop volume in flies) (Wang P et al., 2020). The discovery of the mammalian mechanotransduction channel proteins (PIEZO) in 2010 fueled a rush of mechanotransduction research (Coste et al., 2010). PIEZO receptors have been implicated in sensory transduction across taxa (Coste et al., 2010). In

mammals, PIEZOs mediate touch sensation (through Merkel cells and the nerve cells that innervate them) (Vásquez et al., 2014; Woo et al., 2014), muscle length sensation (through muscle spindles) (Woo et al., 2015b), micturition in the bladder (Marshall et al., 2020), pain sensation and more (Chesler et al. 2016; Zhang et al., 2019).

The two mammalian PIEZO channels (PIEZO1 and PIEZO2) are large (840 kDa) homotrimeric proteins assembled from three ~280kDa monomers. Each monomer contributes to a central nonselective cation channel, and has a peripheral domain that crosses the membrane dozens of times (Soattin et al., 2016). While similar in structure, the two mammalian PIEZO channels have distinct mechanically-activated currents, and are differentially expressed. PIEZO1 is expressed in lungs, bladder, pancreas blood cells, vascular tissue and skin, while PIEZO2 is highly expressed in sensory dorsal root ganglia and other neural tissues (Coste et al., 2010). The exact mechanisms for force transduction in PIEZO receptors are not completely understood. Two different non-exclusive models propose force transduction by PIEZOs: the force-from-lipid and the force-from-filament paradigms (Cox et al., 2017). In the force-from-lipid paradigm the channel is activated by deformations on the associated lipid membrane that surrounds the peripheral propeller part of the channel. Work with PIEZO1 receptors endogenously expressed in different cell types (Romero et al., 2019) and overexpressed in HEK293 cells (Ridone et al., 2020) suggest that these channels indeed operate according to the force-from-lipid paradigm (Syeda et al., 2016). Although PIEZO1 and PIEZO2 channel function is modulated by the plasma membrane (Ridone et al., 2020; Romero et al., 2019), PIEZO2 appears to require an intact cytoskeleton for normal function, lending support to the force-from-filament paradigm. However, it remains unresolved if PIEZO1 requires such cytoskeletal interaction (Eijkelkamp et al., 2013; Romero et al., 2019; Wang J et al., 2020). Functional differences between PIEZO1 and PIEZO2 appear to be the result of differences in the sequence of their beam (i.e., the long helix connecting the blades with the pore domain; Romero et al., 2019). If differences between the transmembrane domains of PIEZO channels contribute to their function and whether these differences lead to distinct patterns of expression is not presently known. However, in mammals, PIEZO2 is differentially spliced to produce at least 16 isoforms with unique properties that are themselves expressed in specific tissues (Szczot et al., 2017).

The nematode *C. elegans* has a single ortholog of PIEZO receptors (*pezo-1*) recently shown to be mechanosensitive (Millet et al., 2021). *pezo-1* has twelve predicted isoforms (a-l, Figure 1A,B). Like PIEZO receptors, PEZO-1 has a highly conserved pore domain and a blade domain comprising 36 (predicted) transmembrane helices (Want et al., 2019). PEZO-1 is expressed throughout the body of *C. elegans*, including the somatic sheath cells and spermathecal cells where it plays an important role in ovulation (Bai et al., 2020). All 12 *pezo-1* isoforms share the conserved pore domain but differ in the number of transmembrane segments associated with the blade component of the channels (Figure 1C). It is not presently known if *pezo-1* isoforms are differentially expressed, or the extent to which they might display functional specializations resembling those seen in the mammalian PIEZO1 and PIEZO2. Using transcriptional and translational reporter strains we found that short *pezo-1* isoforms appear to be primarily expressed in the nervous system while long *pezo-1* isoforms are largely expressed in mesodermal tissues. Long and short isoforms also appear to be differentially expressed in tissues of the digestive system including the pharyngeal gland cells where knock down of long *pezo-1* isoforms expression resulted in loss of food-dependent gland activation. We propose *C. elegans* as an amenable *in vivo* system for the physiological and behavioral study of one of the most complex mechanoreceptors known both at the cellular and whole animal levels. Insights about PEZO-1 isoform function will inform our understanding of the way PIEZO1 and 2 operate in mammals.

**Results:**

The WormBase annotated genome browser identifies up to twelve predicted *pezo-1* isoforms (Figure 1A)(Harris et al., 2020). Protein comparisons of PEZO-1 with human and flies (using Ensembl and aligned nucleotide to protein with BLASTX) returned the human PIEZO1 and PIEZO2, and the *Drosophila* Piezo proteins (Figure 1B) (Harris et al., 2020; Yates et al., 2020). All the isoforms share the C terminus which encodes the conserved pore domain and differ mostly in the number of transmembrane segments within the blade domain of PIEZOs channels (Figure 1C) (Kamajaya et al., 2014). The different isoforms can be divided into long and short isoform groups. The long isoform group comprises the eight longest isoforms (a-h) with over thirty transmembrane segments. The four remaining shorter isoforms (i-l) have between eight and twenty transmembrane segments, and differ in their predicted start sites.

To determine the pattern of expression of different *pezo-1* isoforms we built several transcriptional reporter strains (Figure 1A and Supplementary Table 1). To this end, we selected the putative enhancer regions immediately upstream of the start codon of target isoforms, and used these regions to drive expression of green fluorescent reporter protein (GFP). This approach has been extensively used to report the putative expression of target genes (Boulin et al., 2006) and will be referred to as '*pezo-1* isoform expression' for the purpose of this work.

The putative expression pattern for the longest isoforms (a-h) was assessed using a ~5kb promoter upstream of the gene start codon. There is a large intronic region (>4kb) upstream of isoforms i and j of *pezo-1*. Predicting the presence of an intronic regulatory region, we designed primers targeting isoforms i and j by amplifying the ~5kb intronic region immediately upstream of their predicted start codon (*Ppezo-1*$_{i\text{-}j}$ in Figure 1A). We next constructed a reporter strain using the 5kb upstream of the start codon of isoform k, and similarly another ~5kb promoter sequence immediately upstream of the start codon of isoform l, the shortest predicted isoform (*Ppezo-1*$_k$ and *Ppezo-1*$_l$ respectively). We used standard PCR-fusion (Hobert, 2002) to merge these different putative promoter sequences to GFP and drive fluorophore's expression AVG11 (*Ppezo-1*$_{a\text{-}h}$*::GFP::unc54_3'UTR*), AVG12 (*Ppezo-1*$_{i\text{-}j}$*::GFP::unc54_3'UTR*), AVG23 (*Ppezo-1*$_k$*::GFP::unc54_3'UTR*), and AVG22 (*Ppezo-1*$_l$*:GFP::unc54_3'UTR*). We note that the AVG strains are extrachromosomal and that for each strain we imaged multiple individuals in order to assess mosaicism or variation in array expression. For this study, we report the totality of labelled tissues observed across multiple animals expressing the same array. We found that animals expressing particular constructs showed similar expression patterns, while mosaic animals showed different levels of expression or partial expression.

**Promoter fusion constructs targeting different *pezo-1* isoforms have complementary expressions in gastrointestinal tissues**

GFP expression driven by enhancers targeting different isoforms was detected in tissues associated with the digestive and reproductive systems. However, while expression was largely colocalized to the same organ systems, GFP expression patterns within these organs were distinct for strains targeting different isoforms. Below we provide a description of the tissues we identified as expressing GFP which we imaged using a Leica SP8 confocal microscope.

**Transcriptional reporters targeting *pezo-1*$_{a\text{-}h}$ (long) isoforms**

Using a promoter immediately upstream of the eight longest *pezo-1* isoforms start codon we drove expression of GFP in several mesodermal tissues (Figure 2), including the body wall and pharyngeal muscles, pharyngeal glands and valve, and uterine and defecation tissues. Our findings are consistent with those described by the accompanying manuscript. Based on their morphology and location, we identified GFP expression in pharyngeal muscles (pm3-8), pharyngeal glands (dg1, vg1s, vg2s), pharyngeal-intestinal valve (vpi) cells, AMsh and AMso

glial cells, and the M1 pharyngeal neuron. In addition to our GFP-based extrachromosomal transcriptional reporters, we also used the CRISPR/Cas9 generated AG467 (integrated) strain which tagged mScarlet to the C terminus of PEZO-1 proteins. Imaging of AG467 showed PEZO-1 proteins localized to the vicinity of the pharyngeal grinder, to the quadrants of the pharyngeal bulb occupied by the gland cells, and to the tip of the nose of the worm where the amphid sheath is located. Medially, we saw labelling of the HSN neuron, the vulval muscles, and uterine muscles. Posteriorly, we saw labelling in cells involved in defecation (tentatively identified by their morphology and location as rectD, K, F, B, U, and Y).

**Transcriptional reporters targeting *pezo-1*$_{i\text{-}j}$ (short) isoforms**

Using a promoter immediately upstream of the start codon of *pezo-1* isoforms i and j start codons we drove expression of GFP in pharyngeal muscles and sensory neurons (Figure 3). In the pharynx we saw GFP labeling of the pm3 muscle cells and the mc1 marginal cells within the corpus, a structure responsible for generating suction forces during the ingestion of suspended bacteria (Raizen et al., 2012). A ventral cell located posterior to the terminal bulb and extending a process dorso-anteriorly toward the pharyngeal-intestinal valve was also labelled. In addition to these cells, we found GFP expression in several anterior neurons including the mechanoreceptor FLP and several pharyngeal neurons including cells with morphologies consistent with I6 and M1. Medially, we detected expression in the PVD mechanoreceptor neuron, and more posteriorly a neuron consistent with PVR's morphology and location, as well as other cells associated with the uterus and anus.

**Transcriptional reporters targeting short *pezo-1* isoform expression**

Using a promoter immediately upstream of the start codon of *pezo-1* isoform k to drive GFP expression we saw labelling of the pharyngeal isthmus muscles, the pharyngeal glands, arcade cells, and socket glia (AMso, Figure 4A). In addition, we saw GFP labeling in ventral neurons and in body wall muscles, where it colocalized with our *Pmyo-3::mCherry* body wall co-injection marker (Figure 4B).

We used a promoter region spanning ~5kb upstream of the start codon of the shortest proposed isoform of *pezo-1*, l (Figure 1A, Supplementary Table 2), however, we were unable to detect any resulting GFP expression. This could mean that this proposed isoform does not constitute a real isoform. Alternatively, the promoter region used to drive GFP expression could have missed an important regulatory sequence and thus prevented us from driving GFP expression.

***Long isoforms (pezo-1*$_{a\text{-}h}$) are involved in pharyngeal pumping**

After observing *pezo-1* expression in the pharynx, anal cells, and uterus, we investigated *pezo-1* necessity for processes mediated by these tissues. To this end we used a two-pronged approach. We used RNA interference (RNAi) to reduce *pezo-1* expression in tissues that are non-refractive to RNA (e.g. muscles rather) (Conte et al., 2015, please see note in methods regarding this RNAi clone). Additionally, we used loss of function (LF) and gain of function (GF) mutants generated through CRISPR/cas9.

Wild type animals (N2) treated post-embryonically (L1 through adulthood) with dsRNA targeting *pezo-1*$_{a\text{-}h}$ showed a significantly increased pharyngeal pumping frequency (Figure 5A) when compared to control treatment (L4440) worms. We found that at low food density (A600=0.69), the pharyngeal pumping rates of WT animals were not significantly different than that of animals with loss of function or gain of function mutations on *pezo-1* (Supplementary Figure 1). Our experiments were carried out on standard cultivation plates and *E.coli* (food) concentrations (A600≃0.7). However, worms are known to alter their pharyngeal pumping frequency as a function of food availability (You et al., 2006). To investigate if *pezo-1* plays a role in pharyngeal

responses to changes in food density we allowed worms to feed on bacteria (OP50) diluted to different concentrations. We began by placing worms in a diluted bacterial lawn and transferred them into higher density lawns every 30 minutes. We found that as the bacterial lawn density increased wildtype animals decreased their pharyngeal pumping rate (Figure 5B, black line). However, two *pezo-1* strains with mutations targeting the long (a-h) isoforms displayed impaired abilities to decrease pharyngeal pumping rate when food concentration increased (Figure 5B, gray lines). In a recent manuscript Millet et al. (2021) described a similar impairment for pezo-1 mutants when worms were fed bacteria of increasing sizes.

**Loss of *pezo-1* long isoforms results in abnormal defecation and egg-laying frequencies**

To investigate the potential involvement of *pezo-1* in defecation, we measured pBoc period duration in a *pezo-1* whole-gene knockout (AG405), a whole-gene gain of function mutant (COP1524), and three *pezo-1* long isoform (a-h) knockout mutants (COP1367, COP1553, and AG406). Interestingly, while mutations targeting long *pezo-1* isoforms resulted in shorter defecation periods (i.e. increased frequency), loss of function and gain of function mutations affecting both long and short isoforms had no significant effect on pBoc period (Figure 5C, One-Way ANOVA at the $P<0.5$ level [$F=16.78$, $p<0.001$], followed by multiple comparisons vs control group [Holm-Sidak test] at the $p=0.05$ level)).

We next evaluated the effect of *pezo-1* mutations on egg-laying frequency. Here again we found a difference between whole-gene versus isoform-specific manipulations. Mutations targeting long isoforms of *pezo-1* produced a significant decrease in egg-laying rate (One-Way ANOVA at the $P<0.5$ level [$F=8.72$, $p<0.001$], followed by multiple comparisons vs control group [Holm-Sidak test] at the $p<0.05$ level). Mutations resulting in whole-gene knockout, or a whole-gene gain of function, had a greater effect reducing egg-laying frequency than (Figure 5D, (One-Way ANOVA at the $P=0.5$ level [$F=8.72$, $p<0.001$], followed by pairwise comparisons between COP1367 vs AG405 and COP1524 [Holm-Sidak test] at the $p<0.05$ level).

These results are consistent with normal *pezo-1* expression being important for pharyngeal pumping, defecation, and egg-laying. Furthermore, whole-gene gain and loss of function experiments suggest that loss of one class of isoforms (e.g. long) appears to be more deleterious than loss or gain of function mutations affecting all isoforms equally, hinting perhaps at an antagonistic role for different classes of isoforms in at least some of their functions.

**Measuring activation of pharyngeal gland cells**

The pharyngeal glands are an essential component of food processing, and given the importance of *pezo-1* to pharyngeal pumping, we hypothesized that it may also be involved in regulating pharyngeal gland activity, However, the role of pharyngeal glands during food consumption is not well understood because it is experimentally challenging to assess their activity. To investigate the role of *pezo-1* in pharyngeal gland activity we constructed the AVG09 strain. In this strain a truncated (1.6kb) promoter upstream of the *pezo-1* long isoforms start codon was used to drive GCaMP6s expression in gland cells (as well as uterus and anal cells) without confounding signals from overlaying body wall and pharyngeal musculature (Figure 6). We used this strain to record calcium transients in the pharyngeal gland cells in freely crawling animals to assess pharyngeal gland activation during feeding. One limitation of this approach is that due to the close proximity between pharyngeal gland cells, we were unable to achieve single cell resolution and therefore report the activation status of all five pharyngeal cells together.

**Pharyngeal gland activation decreases as food concentration increases**

In a first step, we characterized normal gland function. As shown above (Figure 5B) pharyngeal pump frequency is reduced when bacterial food density increases. To test whether changes in food density also affected pharyngeal gland activity, we cultured the AGV09 strain in food of different densities and compared GCaMP6 fluorescence across densities. Mirroring the drop in pharyngeal pumping rate, pharyngeal gland cell fluorescence decreased with higher food densities (Figure 6). To ensure that this decrease in fluorescence was not the result of photobleaching we repeated the experiment with different groups of worms feeding bacteria of different density in parallel (rather than sequentially). We obtained a similar drop in fluorescence as before (Supplementary Figure 2), suggesting that gland cell activation indeed decreases with increasing food density.

**_pezo-1$_{a-h}$_ isoforms are involved in food-dependent activation pharyngeal gland cells**

Our results suggest that pharyngeal pumping and pharyngeal gland activation are influenced by the density (concentration) of the bacteria they ingest, suggesting that the presence or absence of food should be reflected in pharyngeal gland activity as well. We found that in non-knocked down animals (i.e. L4440 controls) the brightness of the pharyngeal glands decreased significantly 15 minutes after worms were removed from food (*off food*, Figure 6D red circles). To investigate the potential role of *pezo-1* in the response of the glands to the presence of food we repeated the experiment in *pezo-1$_{a-h}$*-knocked down animals. We found that pharyngeal gland brightness was reduced in the presence of food when compared to control animals and did not significantly change after animals were removed from food for 15 minutes (grey circles in Figure 6D, Two-way ANOVA see Supplementary Table 4 for statistics).

Taken together, we found that knocking down *pezo-1$_{a-h}$* expression increased pharyngeal pumping frequency but lowered pharyngeal gland brightness. Our results thus suggest that both processes are modulated by *pezo-1*, albeit in opposing directions.

**_pezo-1$_{a-h}$_ expression is required for normal passage of food into the intestine**

Our results above showed that knocking down the expression *pezo-1$_{a-h}$* isoforms resulted in increased pharyngeal pumping rate and decreased activation of the pharyngeal gland cells. In *C. elegans*, passage of food from the pharyngeal cavity into the intestinal cavity is mediated by the pharyngeal-intestinal valve, which we found to express long *pezo-1$_{a-h}$* isoforms (Figure 2C). We therefore set out to find out if *pezo-1$_{a-h}$* isoforms were important for the passage of food from the pharynx into the intestine. To visualize food in the digestive tract we used the fluorescent dye DiI as previously described (Vidal-Gadea et al., 2012). Briefly, we mixed OP50 bacteria with the fluorescent dye and allowed control (Figure 7A left) or RNAi-knocked down animals (Figure 7A right) to feed in this mixture for 30 minutes prior to imaging. To assess the efficacy of food movement throughout the gastrointestinal tract, we measured the percentage of the digestive tract where DiI fluorescence could be detected (0 = food absent, 1 = food present throughout the tract). We found no detectable difference in the amount or location of food ingested for wild-type control and knocked down animals (Figure 8C). In both, dye was detected throughout the gastrointestinal tract. However, *pezo-1* is also expressed in some RNAi-refractory cells (such as the M1 neurons). To test whether knocking down expression of long *pezo-1* isoforms in neurons affects valve function, we repeated our experiment in the neuronally sensitized strain TU3311 (Figure 7B left). After knocking down *pezo-1$_{a-h}$* expression in these additional tissues, we observed that food failed to progress into the digestive tract, accumulating instead near the pharyngeal-intestinal valve (Figure 7B right). Quantification of this effect showed that this was a significant effect, demonstrating that neuronal expression of *pezo-1$_{a-h}$* is necessary for ingested food to enter the intestine normally (Figure 7C, two-tailed t-test between animal strains). Investigating the role of *pezo-1* in pharyngeal valve function is beyond the scope of this study and it is the focus of a manuscript in preparation by Dr. Kyuhyung Kim's group.

**Discussion:**

*C. elegans* has a single ortholog (*pezo-1*) of the mammalian PIEZO channels which has a fair amount of conservation with human PIEZO1 and PIEZO2 as well as with the *Drosophila* Piezo channel (Figure 1). The greatest degree of conservation is for the pore domain (Kamajaya et al., 2014). In *C. elegans* up to 12 different isoforms are predicted for *pezo-1* (Harris et al., 2020). This large number of isoforms is consistent with mammals, where PIEZO2, for example, has been shown to be alternatively spliced. The different splice variants of the protein are then expressed in different tissues (Szczot et al., 2017). Alternative splicing of ion channels is also known to occur in *C. elegans (*Johnson et al., 2011). We explored the possibility that different *pezo-1* isoforms may be expressed differentially by using potential enhancer regions upstream of the start codon of single or groups of isoforms to drive GFP expression. We found that constructs targeting long *pezo-1* isoforms (a-h) displayed largely mesodermal GFP expression, similar to PIEZO1 expression in mammals (Hennes et al., 2019). Expression included muscle, gonads, glands, etc. (Figure 2). In contrast, constructs targeting shorter *pezo-1* isoforms resulted in GFP expression in sensory neurons (Figure 3). These results are consistent with findings in mammals, where different isoforms are expressed in different germ layers, suggesting similarly distinct functions for different isoforms in *C. elegans* (Coste et al., 2010).

Our study was not able to target individual isoforms, but rather grouped the longest eight isoforms (a-h) because of their shared start codon. The putative enhancer regions for the remaining (shorter) isoforms (and their predicted start codons) are distributed across a 10kb region. For the purpose of this study, we used a putative enhancer sequence immediately upstream of the i and j isoforms start codon, the k isoform start codon, and the smaller, l, isoform start codon. We designed our promoter sequences trying to maximize the region upstream of the putative isoform start site, while minimizing overlap with other known genes or isoforms. It is, however, possible that our constructs could have erred by either including regulatory sequences belonging to other isoforms, or by neglecting downstream regulatory regions important for the transcription of a targeted isoform. Therefore, tissues identified in this (and similarly designed) work remain putative awaiting cell-specific qPCR validation. Indeed, a CRISPR knock-in strain (AG467) which tags the fluorescent reporter mScarlet at C termini of PEZO-1 and is predicted to encompass all isoforms because of their common stop site shows broader PEZO-1 protein expression than what our transcriptional reporters identified (Bai et al., 2020).

Consistent with the patterns of expression detected above, we found that mutations targeting long isoforms of *pezo-1* expression increased pharyngeal pumping frequencies, while they decreased pharyngeal gland activity. The pharyngeal gland cells are thought to aid in food lubrication and digestion, sending processes to the different pharyngeal compartments (Raharjo et al., 2011). Pharyngeal pumping frequency decreases when worms are migrated from bacteria of low to high nutritional values (You et al., 2006). Therefore, based on our combined results, we propose that *pezo-1* may play a role in discerning the contents of the pharynx. Specifically, in detecting and responding to changes in food density or hardness. Consistent with this idea, in a recent manuscript by the Vásquez lab Millet et al. (2021) reports that *pezo-1* mutants displayed different pharyngeal pumping phenotypes depending on the size of the bacteria they ingested. Similarly, work in *D.melanogaster* recently revealed that the fly's ortholog of PIEZO is involved in the modulation of feeding, with mutations impairing Piezo also resulting in increases in pharyngeal pumping frequency (Wang P et al., 2020).

In addition to pharyngeal pumping, we also found that long *pezo-1* isoforms were required for normal defecation frequency. Specifically, a loss of long isoforms reduced defecation frequency.

However, loss of all isoforms, or gain of function mutation affecting all isoforms, did not have an impact on defecation frequency. These results suggest a potential functional interaction between long and short *pezo-1* isoforms. One interpretation of these findings could be that the increased defecation rate could be a consequence of a faster ingestion of food as a consequence of the increased pharyngeal pumping when long *pezo-1* isoforms are lost. However, the pharyngeal pumping frequencies of these animals were not significantly different under their cultivation conditions (Supplementary Figure 1), which does not support this interpretation. More likely than this idea is that the balance of long and short isoforms is required to maintain correct defecation function.

Unlike pharyngeal pumping and defecation (where loss of *pezo-1* led to increased contraction frequencies), we found that genetic manipulations of *pezo-1* resulted in decreased egg-laying frequencies. A gain of function mutation affecting all isoforms also decreased egg-laying frequency, suggesting that *pezo-1* levels must be carefully regulated to preserve normal egg-laying function. It remains unclear if this effect is related or independent from reports of reduced brood size for *pezo-1* knockout mutants, where brood size in mutants was tightly linked to ovulation (Bai et al., 2020).

Lastly, we found that food passage from the pharynx into the intestine was also impaired when *pezo-1*$_{a\text{-}h}$ expression was reduced through RNAi. Here, however, we found that this effect was only present when long *pezo-1* isoform expression was reduced in a neuronally-sensitized RNAi strain (Figure 7). One caveat here comes from the use of the promoter of *unc-119* to sensitize the neurons of the TU3311 strain to RNAi. While *unc-119* is expressed panneuronally, it is also expressed in a few other tissues (e.g. muscles) and as such the effect of RNA knock down cannot be unambiguously assigned to neural tissues. However, most non-neuronal tissues known to express *unc-119* are also not refractory to RNAi, meaning that such tissues should have undergone a reduction in *pezo-1* expression even in the background (N2) strain. Based on the transcriptional reporter strain results, M1 was the only head neuron labeled with GFP in strains targeting long *pezo-1* isoforms. Ablation of M1 was reported to impair the spitting reflex in worms. It is therefore conceivable that this neuron could play a role in gating passage of food into the intestine (Bhatla et al., 2015). Consistent with this idea, a recent study assigns Piezo an essential role for volume-based control of meal size in *D. melanogaster* (Min et al., 2021).

The role of PIEZO channels in mechanoreception constitutes a new and thriving field of inquiry. It is clear that these channels mediate an extensive array of physiological processes across taxa. In *C. elegans, pezo-1* was implicated in male mating (Brugman, 2020) and ovulation (Bai et al., 2020). The present study represents an initial investigation on the differential expression and function of *pezo-1* isoforms. In the digestive system of *C. elegans pezo-1* enables different organs to independently detect and respond to the presence and quality of food within it. PEZO-1 appears to reflect the mammalian PIEZOs not only in structure, but also in function. *C. elegans* is thus a promising system to study how differences between different PIEZO isoforms endow these channels with the properties that tune them to the different functions, and may inform studies in mammals abou these properties as well.

**Methods and Materials:**

**Animal Strains**

The following strains were used: N2 (WT), AVG09, AVG10, AVG11, AVG12, AVG22, AVG23,TU3311, COP1367, COP1553, COP1524, OH15500, AG405, AG406, AG467. Strains COP1367. COP1553, and COP1524 were a kind gift of Dr. Vásquez at the University of Tennessee. For strain description refer to Supplementary Table 1.

**Statistical analysis**
All the bars report means and variation is given as SEM throughout. All statistical analysis was performed using Sigmaplot 11 (Aspire Software). Comparisons between different experimental groups were performed by planned, two-tailed paired or unpaired t-tests to compare two groups that were normally distributed and had similar variance. One-way ANOVAs were performed between multiple groups. Differences between non-normally distributed groups (or those with unequal variances) were compared using the Mann-Whitney rank-sum test. In all cases, p values are reported following the convention: *p<0.05 and **p<0.001. Please refer to Supplementary Table 4 for summary statistics.

**Bioinformatics**
Protein sequence comparisons were obtained through the protein similarity tool using ENSEMBL (Yates et al., 2020) and incorporated to WormBase (Harris et al., 2020). Functional protein domains were predicted using SMART and GenomeNet Motif search tools (Kanehisa and Sato, 2020; Schultz et al., 2000). We should point out that the widely available RNAi clone targeting *pezo-1* and distributed through the Source Bioscience RNAi library was found to target an incorrect sequence. Source Bioscience provided us with a new, and validated strain (see Supplementary Table 3 targeting the region of the gene consistent with isoforms a through h (N terminus, Figure 1A). This new validated clone is now available through Source Biosciences. While the dsRNA clone targets *pezo-1*$_{a\text{-}h}$ , it does not target the shorter isoforms (i through l).

**Gene knock down**
RNA interference by feeding was conducted as previously described (Conte et al., 2015). Briefly worms were grown in agar plates containing IPTG and seeded with bacteria containing RNAi control vector (L4440), or a vector targeting the gene of interest.

**Filming**
We used a Flea2 camera (Point Grey, Vancouver) mounted on an Olympus SZX12 stereomicroscope to acquire sequences of (1032x776 pixels) TIFF images. Crawling animals were individually filmed at 30Hz for 10 seconds.

**Calcium imaging**
All calcium comparisons were conducted on animals filmed under identical illumination and magnification conditions (alternating strains during the same filming session). Calcium signals were recorded with the aid of an X-cite 120 PC Q light source. We used ImageJ to measure GCaMP6s signals. We measured the brightness of the pharyngeal glands by drawing an area of interest around them and then obtained a background fluorescence measurement by moving the area of interest just outside the worm and measuring this area. We used ImageJ to obtain maximal brightness and reported the ratio of maximal brightness of the pharyngeal glands to the maximal brightness of the background.

**Confocal imaging**
We used a Leica SP8 confocal microscope to acquire 40x image stacks.

**Image analysis**
We used ImageJ to analyze all image sequences.

**Behavioral experiments**
***Pharyngeal pumping.*** Worms were placed in agar plates on OP50 bacterial lawns and allowed to feed for 30 minutes prior to imaging. Animals were filmed using a FlyCap camera (Media Cybernetics) to acquire a series of TIFF images at 10X magnification and 30fps for ten seconds.

A minimum of 30 animals were recorded for each condition. Pharyngeal pumping was measured blind to treatment using ImageJ software.

***Defecation assay.*** We transferred day-1 adult hermaphrodite worms into NGM agar plates seeded with OP50 E.coli and allowed the worms to feed for 30 minutes before imaging. Animals (15 per condition) were imaged at 30fps for 10 minutes. Five consecutive posterior body contractions (pBoc) were measured for each animal. The pBoc period was calculated as the average time between consecutive posterior body contractions. For each strain, we report the average pBoc period of at least ten animals.

***Egg laying assay.*** Egg-laying. The rate of egg laying was assayed by placing ten first-day adult worms in a copper ring (measuring 1.4 cm in diameter) over a bacterial lawn. Worms were allowed to lay eggs for sixty minutes after which they were removed, and the number of eggs counted.

***Food density assay***

We centrifuged 2ml of overnight cultured OP50 *E.coli* for 2 min at 10,000rpm and discarded the supernatant. The bacterial pellet was resuspended in 50 µl of liquid NGM and its optical density at 600nm ($OD_{600}$) was measured using a Thermo Fisher Nanodrop. We made five additional serial dilutions of this stock and measured their optical density as above. A 30 µl drop of each dilution was placed on an NGM agar plate and allowed to dry for 30 minutes. Worms (n=10-15) were transferred into the lowest OP50 density plate and allowed to feed for 30 minutes prior to imaging. Pharyngeal pumping was filmed for each worm as described above. After all worms were filmed they were transferred into the plate with the next higher food concentration and the process was repeated until all the animals were filmed in all food concentrations.

For measuring the activation of the pharyngeal gland cells under different food concentrations we performed the experiments as above but used a fluorescent light to film the pharyngeal gland cells (as described above). Because these animals were reimaged at increasing concentrations, we were concerned that changes in fluorescence could be indicative of fluorophore bleaching rather than changes in cytoplasmic calcium. We therefore repeated this experiment but this time placing 10-15 animals in plates of each food concentration at the same time before filming them. Animals were allowed to feed for 30 minutes before filming with a fluorescent light as described above.

***Food availability assay***

For the food presence assay (10-15) animals were allowed to feed on OP50 *E. coli* lawns on NGM agar plates for 30 minutes. Their pharyngeal pumping (or pharyngeal gland fluorescence) was filmed as described above to produce the “on food 1” condition. The animals were then individually transferred to an NGM agar plate without food for 15 minutes. After this time their pharyngeal pumping (or pharyngeal gland fluorescence) was again filmed to produce the “off food” condition. Animals were then transferred back to a bacterial OP50 lawn where they were filmed one final time within a minute of being reintroduced to produce the “on food 2” condition.

***Food ingestion assay***

Animals (N>100) were fed OP50 *E.coli* mixed with DiI as described above. After 30 minutes of incubation, they were removed and placed in a new OP50 lawn without DiI stain and allowed to rest for 15 minutes before imaging with a fluorescent microscope as described above. Gastrointestinal food occupation was calculated as the ratio of the digestive tract where DiI fluorescence could be detected (measured from mouth to anus using ImageJ) . Occupancy was

therefore reported as a ratio between 0 and 1 where 0 was no fluorescence detected, and 1 was fluorescence detected throughout the entire digestive tract.

**Author contributions:**
HK and VGAG: performed experiments, analyzed data, wrote manuscript. SA: performed experiments. AJ: constructed strains. XB: performed experiments, constructed strains, analyzed data. RB: performed experiments, analyzed data. JJ: performed experiments. BC: constructed strains. HE, FA, FP, MS, FEM: constructed experiments. BM, SW: wrote manuscript.

**Acknowledgements**
Some strains were provided by the Caenorhabditis Genetics Center (funded by NIH Grant P40 OD010440). Funding was provided by NIH Grant 1R15AR068583-01A1, and NSF Grant 1818140 to A.G.V.-G. This work was supported, in part, by the Intramural Research Program of the National Institutes of Health, National Institute of Diabetes and Digestive and Kidney Diseases (X.B., R.B). We thank Dr. Andy Golden for feedback on the manuscript. We thank Dr. Valeria Vásquez for the worm strains.

**Figure Captions**
**Figure 1.** Genetic map of *C. elegans' pezo-1*. **A)** Wormbase (Harris et al., 2020) diagram of *pezo-1* showing twelve predicted isoforms (a-l). Exons are shown in blue boxes separated by introns (black lines). The two 5kb sequences used to drive expression of GFP are shown targeting a-h isoforms (top left black bar), i-j, k, and l isoforms (top black bars). Also highlighted is the abbreviated promoter sequence used to drive GCaMP6s expression in the pharyngeal gland cells (red bar), as well as the coding sequence targeted by RNA interference (green bar). The black verticals arrows denote the sites of mutations on different isoforms are mapped to the different strains obtained from the Million Mutation Project (Thompson et al., 2013). **B)** Protein similarity regions between the worm PEZO-1 and the human PIEZO1 and PIEZO2 (PIEZO1: score=100, E-val=4e-17, %ID=32.7; PIEZO2: score=82, E-val=1e-11, %ID=58.33), and the fruit fly Piezo (score=666, E-val=0.0, %ID=27.8) obtained from WormBase through ENSEMBL ,and BLASTX (Yates et al., 2020; Harris et al., 2020). The bars are shown in alignment to the gene sequence in A. **C)** Functional protein domain analysis obtained through SMART and GenomeNet Motif showing the predicted location of the cation channel (red) and the transmembrane domains that constitute the propeller blade domains of the channel (Kanehisha et al., 2020; Schultz et al., 2000). The different isoform groups are aligned to show the predicted transmembrane domains present in each group (black lines).

**Figure 2.** The *pezo-1*$_{a\text{-}h}$ isoforms are expressed in distinct gonad and digestive tract and associated tissues. **A)** A 5kb promoter upstream of the *pezo-1* start site was used to drive expression of GFP targeting long isoform expression. **B)** Long *pezo-1* isoforms (a-h) were expressed in pharyngeal gland cells (dorsal and ventral g1), and the AMso glia. **C)** GFP was also present in ventral pharyngeal gland cells (vg2), the intestinal valve, and **D)** the Amsh glia. **E)** Cells with consistent anatomy and location with the pharyngeal neuron I6 were labelled. **F)** The pharyngeal neuron M1 and body wall musculature also expressed GFP. Pharyngeal muscles including the isthmus and terminal bulb (pm3, and pm5-8) were labelled in most preps. **G)** We saw *pezo-1* expression in the uterus and vulva, as well as in the HSN neuron. The AG467 translational reporter strain tagging the N-terminus of *pezo-1* proteins (PEZO-1::mScarlet) shows PEZO-1 protein accumulation in the vulva and vulval muscles **(i)**. **H)** *pezo-1* expression was detected in several cells associated with defecation, including cells K, F, B, U, Y, and rectD. **I)** The translational reporter strain targeting the domain shared between all isoforms showed expression consistent with our transcriptional reporters, with obvious protein accumulation in regions consistent with the glial terminal processes **(a)**, pharyngeal glands **(b)**,

and pharyngeal grinder **(c)**. Animals are presented in sagittal views (dorsal up, anterior left) with the exception of F (partial coronal projection). All scale bars are 10μm unless otherwise indicated. All images were obtained using a Leica SP8 white light laser confocal microscope.

**Figure 3.** The *pezo-1*$_{ij}$ isoforms are expressed in the gonad and digestive tract and associated tissues. **A)** 4.9kb promoter spanning the largest intron in the *pezo-1* gene was used to drive GFP expression of the shorter *pezo-1* isoforms (using coelomocyte::GFP as coinjection marker). **B)** GFP expression was present in pharyngeal muscles 3 (pm3), the marginal cells 1 (mc1) of the procorpus, and the anterior mechanosensitive neuron PVD. **C)** Expression was seen in a pharyngeal neuron consistent with I6. **D)** Expression was also detected in PHC,and the mechanosensitive neurons PVD **(E)**. **F)** An anterior ventral cell projecting to the intestinal valve was also labelled (*). **G)** Unlike GFP expression driven by the long isoform promoters, fluorescence signals were evident in late embryos. **H)** These expression patterns were confirmed by the PEZO-1::mScarlet (red) strain using magenta to tag the C-terminal end of all PEZO-1 proteins. All scale bars are 10μm unless otherwise indicated. Animals are presented in sagittal views (dorsal up, anterior left). All images were obtained using a Leica SP8 white light laser confocal microscope.

**Figure 4.** The *pezo-1*$_k$ isoform was expressed in pharyngeal and neural tissues. **A)** *pezo-1*$_k$ was observed in several pharyngeal tissues including the pharyngeal glands, pharyngeal isthmus, arcade cells, the pharyngeal valve, AMso cells, and some pharyngeal neurons. **B)** *pezo-1*$_k$ was also expressed in body wall muscles and several ventral neurons. Green is *Ppezo-1k::GFP*, red is *Pmyo-3::mCherry*. Scale bar is 50μm. All images were obtained using a Leica SP8 white light laser confocal microscope.

**Figure 5.** Long *pezo-1* isoforms are required for normal pharyngeal response to increases in food density . **A)** knock down (by feeding) of *pezo-1*$_{a-h}$ expression in a wildtype (N2) background resulted in an increase in pharyngeal pumping frequency (t-test, N=30). **B)** Cultivation of WT (N2) *C. elegans* in bacteria of increasing densities resulted in a decrease in pharyngeal pumping rate (blue line). However, mutations affecting long isoforms of pezo-1 resulted in worms that displayed an impaired response to food density increases (red line: 6.6kb deletion of 5' end of pezo-1; green line: 198bp deletion plus 23bp insertion on first exon). **C)** Mutations resulting in loss of long *pezo-1* isoforms caused a decrease in pBoc period duration. However, loss of function and gain of function mutations affecting all isoforms of *pezo-1* had no effect on pBoc period duration. **D)** Mutations affecting long pezo-1 isoform resulted in a significant reduction in egg-laying rates. Loss of function, and gain of function mutations affecting all pezo-1 isoforms caused an even greater reduction in egg-laying rates. (C-D) One-Way ANOVA Pairwise Multiple Comparison Procedures (Holm-Sidak method), Kruskal-Wallis test, *p<0.05, **p<0.001.

**Figure 6.** Pharyngeal gland cells respond to the presence of food in a *pezo-1* dependent manner. **A)** A short (1.6kb) *pezo-1* promoter was used to drive expression of the calcium reporter GCaMP6s in pharyngeal gland cells in the strain AGV09. This allowed gland cells to be visible without obstruction by the body wall musculature (and other overlying *pezo-1*$_{a-h}$-expressing tissues). **B)** Increasing food density resulted in decreased pharyngeal pumping frequency, and in a decrease in gland cell brightness **(C)**. **D)** Animals were allowed to feed for 30 minutes (*on food 1*), transferred to plates without food for 15 minutes (*off food*), and reintroduced into plates with food once again (*on food 2*). The average relative brightness of pharyngeal gland cells in control animals (red circles) decreased significantly when worms were removed from food for 15 minutes (*off food*). Knock down *pezo-1*$_{a-h}$ isoform expression

abolished brightness changes gland cells associated with removal from food (grey circles). Two-Way ANOVA, Holm-Sidak pairwise comparison at p<0.05; N=9-12; a=p<0.05 (*pezo-1* RNAi treated vs L4440 controls), b=p<0.05 (L4440: *off food* and *on food 2* treatments vs *on food 1* treatment). Please refer to Supplementary Table 4 for statistics.

**Figure 7.** Neuronal expression of *pezo-1* mediates food transport into the intestine.To investigate how *pezo-1* mediates food intake, we fed worms OP50 bacteria fluorescently stained with DiI. **A)** Compared to animals fed a control construct (L4440), RNAi knock down of *pezo-1*$_{a\text{-}h}$ isoform expression in a wildtype background did not appear to affect food intake. **B)** knock down *pezo-1*$_{a\text{-}h}$ isoform expression in a neuronally-sensitized RNAi strain reduced the amount of food entering the intestine compared to controls. **C)** Fraction of the digestive tract (buccal cavity to anus) occupied by fluorescent food following 15 minutes of feeding in control (L4440), and *pezo-1*-knocked down animals in both a wildtype (N2) and a neuronally-sensitized RNAi strain (TU3311). N=20, paired, 2-tailed t-test ** p<0.01.

## Supplementary Information

## Supplementary Figure Captions.

**Figure Supplementary 1.** Genetic manipulation of *pezo-1* does not result in impaired pharyngeal pumping frequency in worms feeding in law density food. Cultivation of *C. elegans* worms in OP50 of A600=0.69 resulted in high pharyngeal pumping frequencies in WT (N2) worms (red bar). CRISPR/Cas9 mutations resulting in whole-gene (black bar) and long isoform (grey bars) loss of function mutations did not alter pharyngeal pumping frequencies. Similarly, Whole-gene gain of function mutations (white bar) did not affect pharyngeal frequency.

**Figure Supplementary 2.** Increasing food density caused the brightness of the pharyngeal gland cells to decrease. NGM agar plates were seeded with a 30 µl lawn of OP50 *E.coli* bacteria at four different densities. Wild type animals (AVG09, n>10) were then placed into each plate and allowed to feed for 30 minutes. After this, pharyngeal gland cells were filmed and their brightness measured and normalized against their background.

## Supplementary Tables

**Supplementary Table 1.** Animal strains used in this study.

| Strain | Allele | Position | Mutation/genotype | Description |
|---|---|---|---|---|
| N2 | n/a | n/a | WT | Reference strain |
| TU3311 | n/a | unknown | *uIs60 [unc-119p::YFP + unc-119p::sid-1]* | Hypersensitive neuronal RNAi |
| COP1367 | knu384 | IV:9366441 | *pezo-1* (knu384 - 198bp deletion and 23bp insertion): gaatcggtggtcgtaacacagcaacaacaga//ATGACGGTCCCGCC - deletion of 198bp and insertion of ACAGCAACAACAGAATGACGGTC - TCGAAAGTCTTTAGCACTTCCCAgtaagaaattaaagtccgatgt | leads to premature stop - MTVPPQQQQNDGLESL* |
| COP1524 | knu490 | IV:9366455 | *pezo-1* GOF: R2373K (based on isoform G amino acid residues sequence) | Gain of function mutation affecting all isoforms. |
| COP1553 | knu508 | unknown | *pezo-1* 6,616bp deletion | 6.6kb deletion at 5' end of gene affects 8 longest isoforms (a-h) |
| AG405 | av143 | unknown | *pezo-1* C-terminus deletion of Exon 27-33 + introns, generated by CRISPR/Cas9, Inserted STOP CODON AFTER deletion | Deletion affecting 8 longest isoforms (a-h) |
| AG406 | av144 | unknown | *pezo-1* N-terminus deletion of Exon 1-13 + introns, generated by CRISPR/Cas9, Inserted STOP CODON AFTER deletion | Deletion affecting all isoforms of *pezo-1* |

| | | | | |
|---|---|---|---|---|
| AG467 | av182 | n/a | *pezo-1(av182 [pezo-1::mScarlet]) IV*; CRISPR/Cas9 edit | mScarlet in C terminus generated through CRISPR/Cas9 |
| AVG09 | ury09 | n/a | *uryEx09[Ppezo-1::GCaMP6s::unc54_3'UTR, Pmyo-3::mCherry::unc54_3'UTR]* | GCaMP6s in pharyngeal glands, gonad and anal cells, red bodywall |
| AVG10 | ury10 | n/a | *uryEx10[Ppezo-1ah::GFP::unc54_3'UTR, Pmyo-3::mCherry::unc54_3'UTR]* | GFP *pezo-1* a-h isoforms, red bodywall |
| AVG11 | ury11 | n/a | *uryEx11[Ppezo-1ij::GFP::unc54_3'UTR, Pcoel::GFP::unc54_3'UTR]* | GFP *pezo-1* i and j isoforms, GFP in coelomocyte |
| AVG23 | ury12 | n/a | *uryEx12[Ppezo-1k::GFP::unc54_3'UTR, Pmyo-3::mCherry::unc54_3'UTR]* | GFP *pezo-1* isoform k, mCherry in body wall muscles |
| AVG22 | ury13 | n/a | *uryEx13[Ppezo-1l::GFP::unc54_3'UTR, Pcoel::GFP::unc54_3'UTR]* | GFP *pezo-1* isoform l, GFP in coelomocyte |

**Supplementary Table 2.** Primers used for the construction of strains used in this study.

| **Primer** | **Sequence (5'-3')** | **location** | **Product** |
|---|---|---|---|
| *Ppezo-1* a-h FWD | CATTCAAAAGGAAGAGGCAGA | IV: 9371411 | |
| *Ppezo-1* a-h REV | CTGAACAATCGCCGAGAAATCAAG | IV: 9366539 | 4,872bp |
| *Ppezo-1* i-j FWD | TTGCAAAGTTCCCATGGTTT | IV: 9360555 | |
| *Ppezo-1* i-j REV | GTCGATGGAGCTGATGTTGA | IV: 9355693 | 4,862bp |
| *Ppezo-1GCAMP6s* FWD | GGCGCGTCGAGACCT | IV: 9368065 | |
| *Ppezo-1GCAMP6s* REV | TCTGTTGTTGCTGTGTTACGA | IV: 9366455 | 1,610bp |
| *Ppezo-1* k FWD | TTGCTCGCACAGTAGAATAGAAC | IV: 9364926 | |
| *Ppezo-1* k REV | TGCTCTTCTTGGTGACGTTG | IV: 9359527 | 5,399bp |
| *Ppezo-1* l FWD | GCGATACCCTTGTCAAGAAGC | IV: 9353590 | |
| *Ppezo-1* l REV | GACCCCATGAACACCAAATC | IV: 9348570 | 5,020bp |

**Supplementary Table 3.** Sequencing results from Source Bioscience for their new *pezo-1* RNAi clone (top), and alignments of the sequence to *C. elegans* genome (bottom) obtained through WormBase through ENSEMBL and BLASTX (Yates et al., 2020; Harris et al., 2020).

NNNNNNNNNNNNNNNNNNACTCCNNNAGGGNGNNNNCAGATCTGATTGAGTGGGAACGATCGGAATTTGAT
ATGTGTAGAGAACCAAGAAATGAAGCGCCGAGTAGAATATGAGAAACTGAAAATATCGAAAAGGTTTTACAGATA
AATTTCGTACCGCCCATACCTTCTTTATCTGATTGTACACTCCATGTCTCAGTGGTGTGTATGTGGACCACCACG
TGGATATGAACAGAAAAGCGAGAAAGTAAATTGAGTTACTCAGCGATGGTTTCACGATTCCAACATATGCCGTG
AACAGGAAAAGCACGAAATTAGTCAATCTTCGTAGAGAATTTCCGATTGCACTCCACATTATAGCGGCTAACTTT
CTTTGTCGTCGTTGCTCGCGGCCACTGAAATAGTTAATATATTATTTGAGTTCATAAGTATATTCTAACGCACGATT
CACTCCTGACTGTTACAACATCACCAACGACGTCCAATTGCTCGTCTCTATGCGACAAAAACATGACGATTATGA
TAGTGAGCAGAGCTGCAGACGTGGCAATAATCTCCGGAAGAAATGCTCGAGTTGATTCAAATGTTCCTGTTGGA
TGGAATCGGACAAGGCCAATGCTCCGGAACAGAGTAGTGTCGGATCGATTGCAAATGTATGTCCGGTCTTTTTT
ATGAACAACTTGTTCTGAGATCTGTAANATAATATTTAATCAACTGTTTCATAANCTATTTTTACCTGGNAGGAACC
AACTCCTAGTGCGACTGCTAGGCAGAAGAGAAAAGTGATAATANCGAATGTNCCAACTAGTTNTNNNAAAGAAT
ATTGATTTCAACGACNTCNNACTTTAATTTCTTACNGGGAAGTGCTAAANACTTTCGAATTGGTGGNAAANCGG
CNCTGACAAGTGCAAGTAGNACNTANCCAATTGNTAAAAAGCTCGCCGGTTTATGGGCAGCTGAAAAANTTGA
GCNTTANNNTNTACTANNTTNNGGAAACACCTGTTNAAATGAAANAAAANNNAGCTANCCTGCNANNNGTGCT
GCCNGATAGCAGCANTTTGANNANNGCANNATTNNAAAAGNCGGCNNGNCCNNCTATCNGTNNNNNNTGGNN
NNNCNNCCCCCGNATNCNNNNNNNANCNNANNATNNNANNNTNNTCNNNNCCNNCNNCNNNNNNNNGGGGG
NNGACCNNNTNNCCCNN

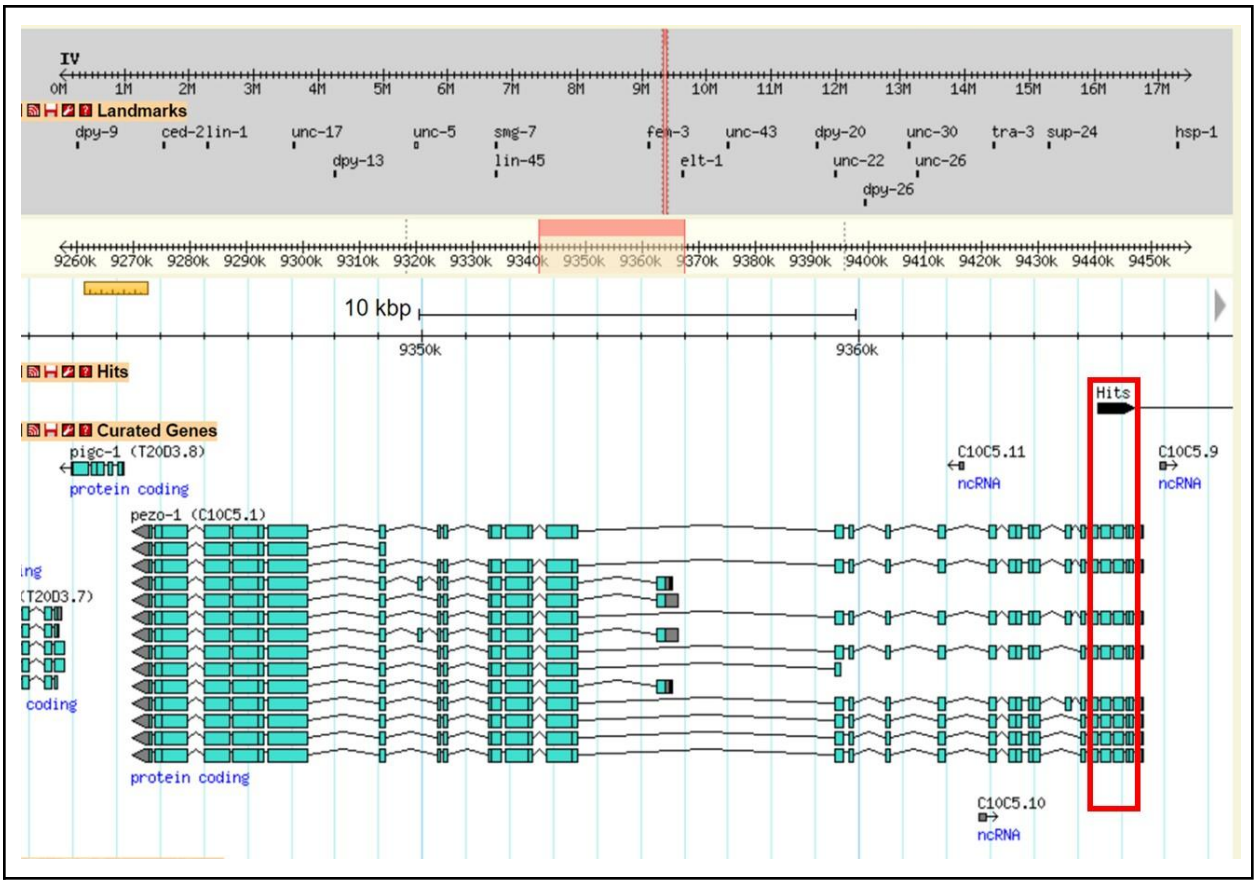


**Supplementary Table 4.** Statistical tests used for the different comparisons made in this study. Tests used and sample sizes (for each treatment) for the figures presented in this paper

| Figure | Statistic test | N | Significance |
|---|---|---|---|
| Figure 5A | Mann-Whitney Rank Sum Test | 30 | **p<0.001 |
| Figure 5B | N2 $r^2$=0.55; AG405 $r^2$=0.45; COP1367 $r^2$=0.19; COP1553 $r^2$=0.10; AG406 $r^2$=0.37; COP1524 $r^2$=0.38 | >10 | |
| Figure 5C | One-Way ANOVA Pairwise Multiple Comparison Procedures (Holm-Sidak method), Kruskal-Wallis test. F16.8; DF5 | 10 | **p<0.001 |
| Figure 5D | One-Way ANOVA Pairwise Multiple Comparison Procedures (Holm-Sidak method), Kruskal-Wallis test. F=8.7; DF=5 | >10 | *p<0.05, **p<0.001 |
| Figure 6B | $r^2$=0.37 | 10-15 | |
| Figure 6C | $r^2$=0.22 | 10-15 | |
| Figure 6D | Two-Way ANOVA, RNAi F=53.6, Fed F=9.8, RNAixFed F=12.6 at p<0.001; Holm-Sidak pairwise comparison at p<0.05 | 9-12 | a= p<0.05 (pezo-1 vs L4440)<br>b= p<0.05L (4440 off food and on food 2 vs on food 1) |
| Figure 7C | Mann-Whitney Rank Sum Test | 109 | **p<0.001 |
| SuppFig 1 | One-Way ANOVA | 10 | *p<0.05, **p<0.001 |
| SuppFig 2 | $r^2$=0.32 | 12-15 | |

## Reference


Bai, X., Bouffard, J., Lord, A., Brugman, K., Sternberg, P.W., Cram, E.J., and Golden, A. (2020). Caenorhabditis elegans PIEZO channel coordinates multiple reproductive tissues to govern ovulation. Elife *9*.

Bhatla, N., Droste, R., Sando, S.R., Huang, A., and Horvitz, H.R. (2015). Distinct Neural Circuits Control Rhythm Inhibition and Spitting by the Myogenic Pharynx of C. elegans. Curr Biol *25*, 2075-2089.

Boulin, T. et al. Reporter gene fusions. (2006), WormBook, ed. The *C. elegans* Research Community, WormBook, doi/10.1895/wormbook.1.106.1, http://www.wormbook.org.

Brugman, K.I. (2020) *pezo-1* function in *Caenorhabditis elegans*. Dissertation (Ph.D.), California Institute of Technology. doi:10.7907/fz4z-c850

Chesler, Alexander T., et al. "The role of PIEZO2 in human mechanosensation." New England Journal of Medicine 375.14 (2016): 1355-1364.

Conte, D., Jr., MacNeil, L.T., Walhout, A.J.M., and Mello, C.C. (2015). RNA Interference in Caenorhabditis elegans. Curr Protoc Mol Biol *109*, 26 23 21-26 23 30.

Coste, B., Mathur, J., Schmidt, M., Earley, T.J., Ranade, S., Petrus, M.J., Dubin, A.E., and Patapoutian, A. (2010). Piezo1 and Piezo2 are essential components of distinct mechanically activated cation channels. Science *330*, 55-60.

Cox, C.D., Bavi, N., and Martinac, B. (2017). Origin of the Force: The Force-From-Lipids Principle Applied to Piezo Channels. Curr Top Membr *79*, 59-96.

Currie, S.N. (1991). Vibration-evoked startle behavior in larval lampreys. Brain Behav Evol *37*, 260-271.

Eijkelkamp, N., Linley, J.E., Torres, J.M., Bee, L., Dickenson, A.H., Gringhuis, M., Minett, M.S., Hong, G.S., Lee, E., Oh, U.*, et al.* (2013). A role for Piezo2 in EPAC1-dependent mechanical allodynia. Nat Commun *4*, 1682.

Harris, T.W., Arnaboldi, V., Cain, S., Chan, J., Chen, W.J., Cho, J., Davis, P., Gao, S., Grove, C.A., Kishore, R.*, et al.* (2020). WormBase: a modern Model Organism Information Resource. Nucleic Acids Res *48*, D762-D767.

Hennes, A., Held, K., Boretto, M., De Clercq, K., Van den Eynde, C., Vanhie, A., Van Ranst, N., Benoit, M., Luyten, C., Peeraer, K.*, et al.* (2019). Functional expression of the mechanosensitive PIEZO1 channel in primary endometrial epithelial cells and endometrial organoids. Sci Rep *9*, 1779.

Hobert, O. (2002). PCR fusion-based approach to create reporter gene constructs for expression analysis in transgenic C. elegans. Biotechniques *32*, 728-730.

Kamajaya, A., Kaiser, J.T., Lee, J., Reid, M., and Rees, D.C. (2014). The structure of a conserved piezo channel domain reveals a topologically distinct beta sandwich fold. Structure *22*, 1520-1527.

Kanehisa, M., and Sato, Y. (2020). KEGG Mapper for inferring cellular functions from protein sequences. Protein Sci *29*, 28-35.

Katoh, E., Sbragaglia, V., Aguzzi, J., and Breithaupt, T. (2013). Sensory biology and behaviour of Nephrops norvegicus. Adv Mar Biol *64*, 65-106.

Liu, L., Li, Y., Wang, R., Yin, C., Dong, Q., Hing, H., Kim, C., and Welsh, M.J. (2007). Drosophila hygrosensation requires the TRP channels water witch and nanchung. Nature *450*, 294-298.

Marshall, K.L., Saade, D., Ghitani, N., Coombs, A.M., Szczot, M., Keller, J., Ogata, T., Daou, I., Stowers, L.T., Bonnemann, C.G.*, et al.* (2020). PIEZO2 in sensory neurons and urothelial cells coordinates urination. Nature.

Min, S., Oh, Y., Verma, P., Whitehead, S.C., Yapici, N., Van Vactor, D., Suh, G.S. and Liberles, S. (2021). Control of feeding by Piezo-mediated gut mechanosensation in *Drosophila*. Elife, 10, p.e63049.

Murthy, S.E., Loud, M.C., Daou, I., Marshall, K.L., Schwaller, F., Kuhnemund, J., Francisco, A.G., Keenan, W.T., Dubin, A.E., Lewin, G.R., *et al.* (2018). The mechanosensitive ion channel Piezo2 mediates sensitivity to mechanical pain in mice. Sci Transl Med *10*.

Raharjo, W.H., Ghai, V., Dineen, A., Bastiani, M., and Gaudet, J. (2011). Cell architecture: surrounding muscle cells shape gland cell morphology in the Caenorhabditis elegans pharynx. Genetics *189*, 885-897.

Raizen D., Song B., Trojanowski N. and You Y. Methods for measuring pharyngeal behaviors (December 18, 2012), WormBook, ed. The *C. elegans* Research Community, WormBook, doi/10.1895/wormbook.1.154.1, http://www.wormbook.org.

Ridone, P., Pandzic, E., Vassalli, M., Cox, C.D., Macmillan, A., Gottlieb, P.A., and Martinac, B. (2020). Disruption of membrane cholesterol organization impairs the activity of PIEZO1 channel clusters. J Gen Physiol *152*.

Romero, L.O., Massey, A.E., Mata-Daboin, A.D., Sierra-Valdez, F.J., Chauhan, S.C., Cordero-Morales, J.F., and Vasquez, V. (2019). Dietary fatty acids fine-tune Piezo1 mechanical response. Nat Commun *10*, 1200.

Rosenbaum, T., Benitez-Angeles, M., Sanchez-Hernandez, R., Morales-Lazaro, S.L., Hiriart, M., Morales-Buenrostro, L.E., and Torres-Quiroz, F. (2020). TRPV4: A Physio and Pathophysiologically Significant Ion Channel. Int J Mol Sci *21*.

Schultz, J., Copley, R.R., Doerks, T., Ponting, C.P., and Bork, P. (2000). SMART: a web-based tool for the study of genetically mobile domains. Nucleic Acids Res *28*, 231-234.

Soattin, L., Fiore, M., Gavazzo, P., Viti, F., Facci, P., Raiteri, R., Difato, F., Pusch, M., and Vassalli, M. (2016). The biophysics of piezo1 and piezo2 mechanosensitive channels. Biophys Chem *208*, 26-33.

Syeda, R., Florendo, M.N., Cox, C.D., Kefauver, J.M., Santos, J.S., Martinac, B., and Patapoutian, A. (2016). Piezo1 Channels Are Inherently Mechanosensitive. Cell Rep *17*, 1739-1746.

Szczot, M., Pogorzala, L.A., Solinski, H.J., Young, L., Yee, P., Le Pichon, C.E., Chesler, A.T., and Hoon, M.A. (2017). Cell-Type-Specific Splicing of Piezo2 Regulates Mechanotransduction. Cell Rep *21*, 2760-2771.

Thompson, O., Edgley, M., Strasbourger, P., Flibotte, S., Ewing, B., Adair, R., Au, V., Chaudhry, I., Fernando, L., Hutter, H., *et al.* (2013). The million mutation project: a new approach to genetics in Caenorhabditis elegans. Genome Res *23*, 1749-1762.

Vásquez, V., Scherrer, G., and Goodman, M.B. (2014). Sensory biology: it takes Piezo2 to tango. Curr Biol *24*, R566-R569.

Vidal-Gadea, A.G., Davis, S., Becker, L., and Pierce-Shimomura, J.T. (2012). Coordination of behavioral hierarchies during environmental transitions in Caenorhabditis elegans. Worm *1*, 5-11.

Wang, J., Jiang, J., Yang, X., Wang, L., Xiao, B. (2020). Tethering Piezo channels to the actin cytoskeleton for mechanogating via the E-cadherin-β-catenin mechanotransduction complex. bioRxiv DOI: https://doi.org/10.1101/2020.05.12.092148

Wang, P., Jia, Y., Liu, T., Jan, Y.N., and Zhang, W. (2020). Visceral Mechano-sensing Neurons Control Drosophila Feeding by Using Piezo as a Sensor. Neuron *108*, 640-650 e644.

Woo, S.H., Lukacs, V., de Nooij, J.C., Zaytseva, D., Criddle, C.R., Francisco, A., Jessell, T.M., Wilkinson, K.A., and Patapoutian, A. (2015b). Piezo2 is the principal mechanotransduction channel for proprioception. Nat Neurosci *18*, 1756-1762.

Woo, S.H., Ranade, S., Weyer, A.D., Dubin, A.E., Baba, Y., Qiu, Z., Petrus, M., Miyamoto, T., Reddy, K., Lumpkin, E.A., *et al.* (2014). Piezo2 is required for Merkel-cell mechanotransduction. Nature *509*, 622-626.

Yates, A.D., Achuthan, P., Akanni, W., Allen, J., Allen, J., Alvarez-Jarreta, J., Amode, M.R., Armean, I.M., Azov, A.G., Bennett, R., *et al.* (2020). Ensembl 2020. Nucleic Acids Res *48*, D682-D688.

You, Y.J., Kim, J., Cobb, M., and Avery, L. (2006). Starvation activates MAP kinase through the muscarinic acetylcholine pathway in Caenorhabditis elegans pharynx. Cell Metab *3*, 237-245.

Zhang, M., Wang, Y., Geng, J., Zhou, S., and Xiao, B. (2019). Mechanically Activated Piezo Channels Mediate Touch and Suppress Acute Mechanical Pain Response in Mice. Cell Rep *26*, 1419-1431 e1414.

## Figures

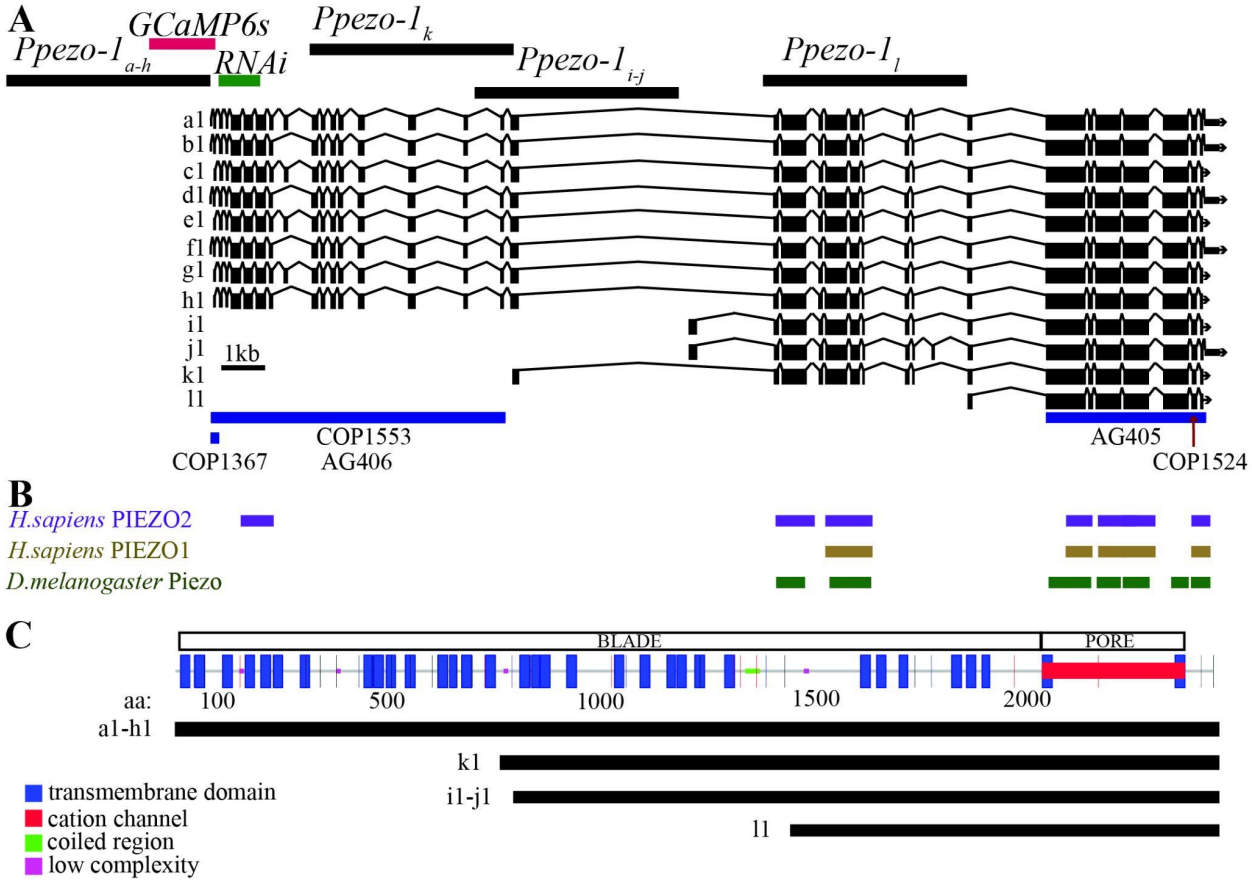


**Figure 1**

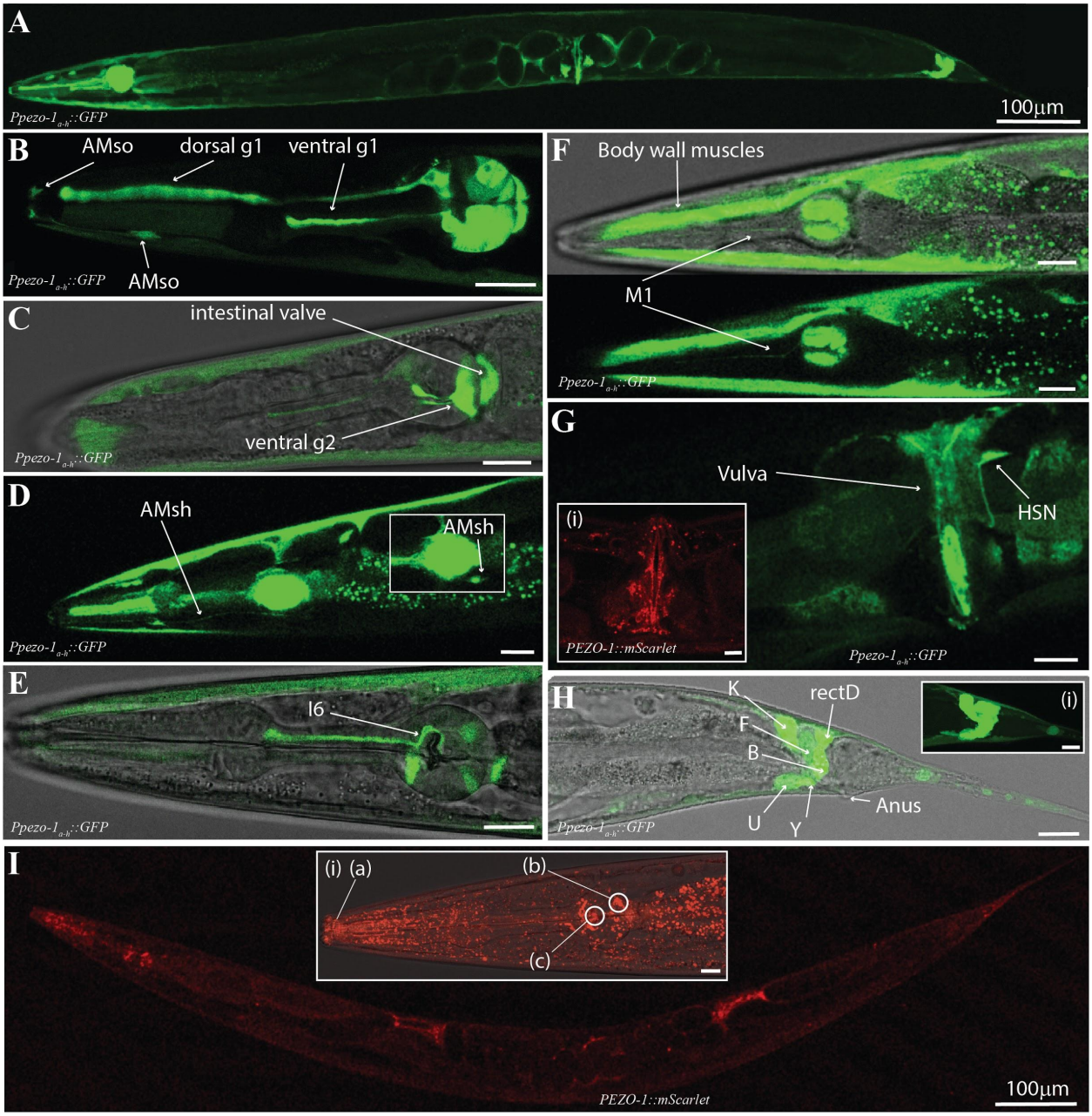


**Figure 2.**

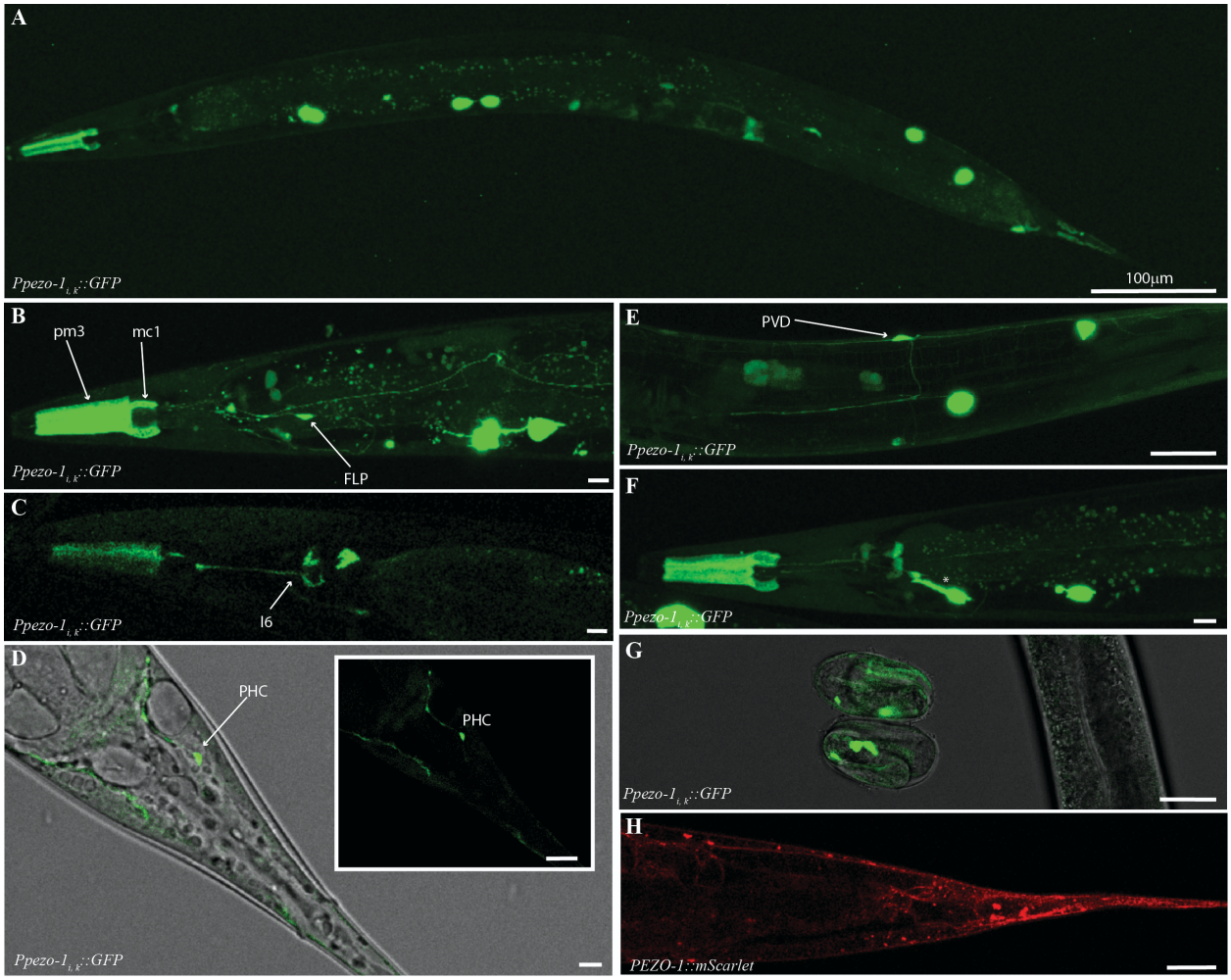


**Figure 3.**

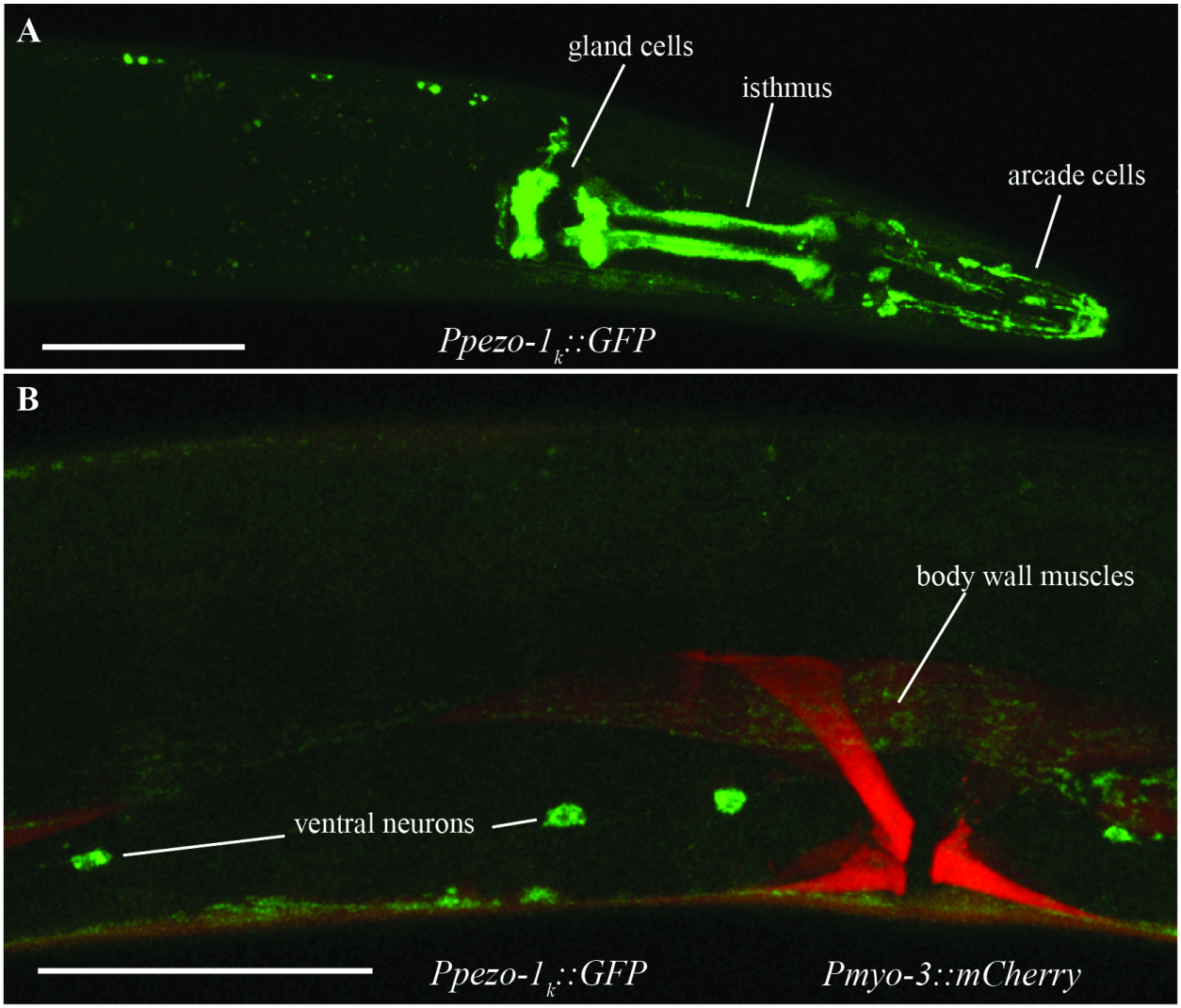


**Figure 4**

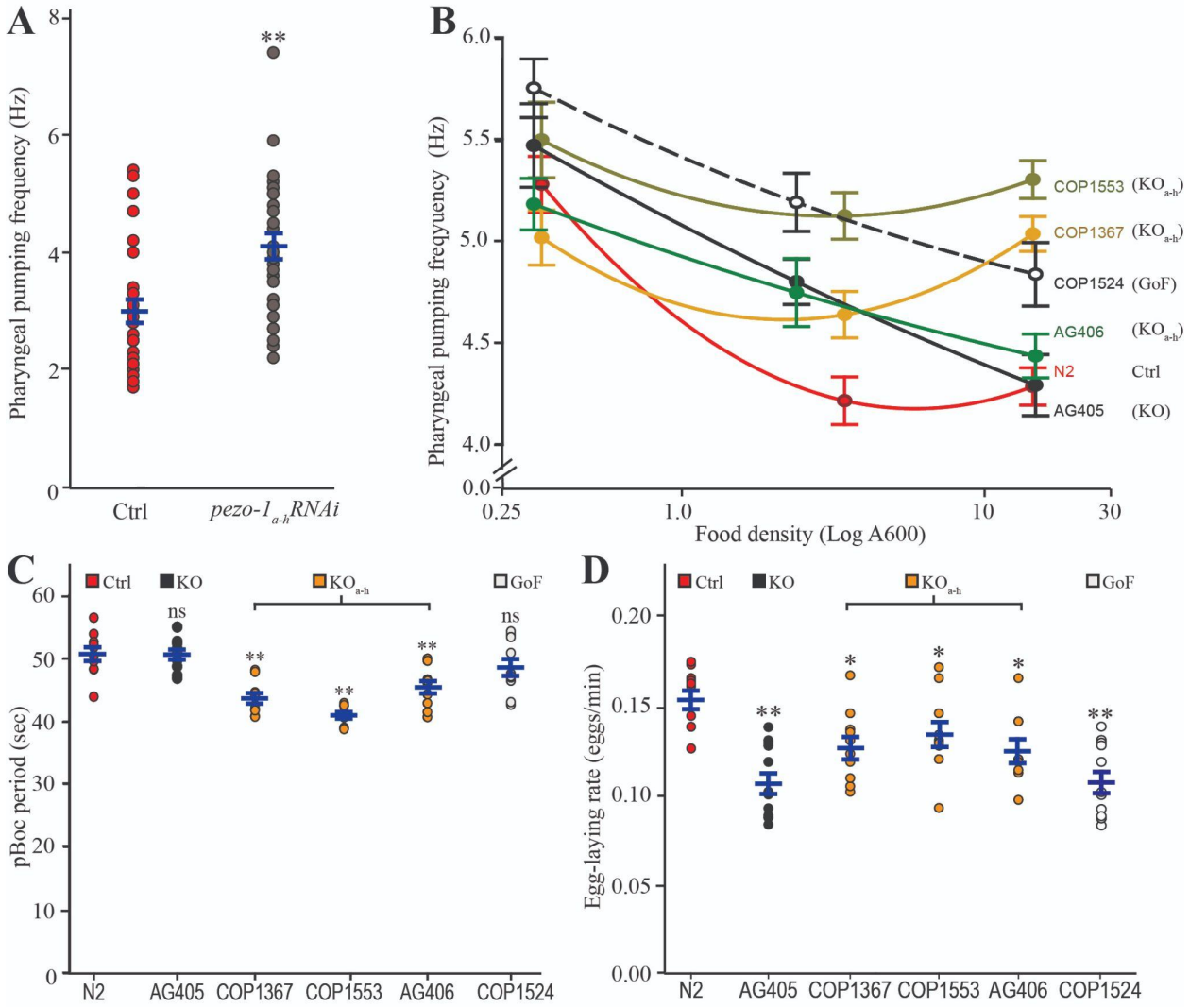


**Figure 5**.

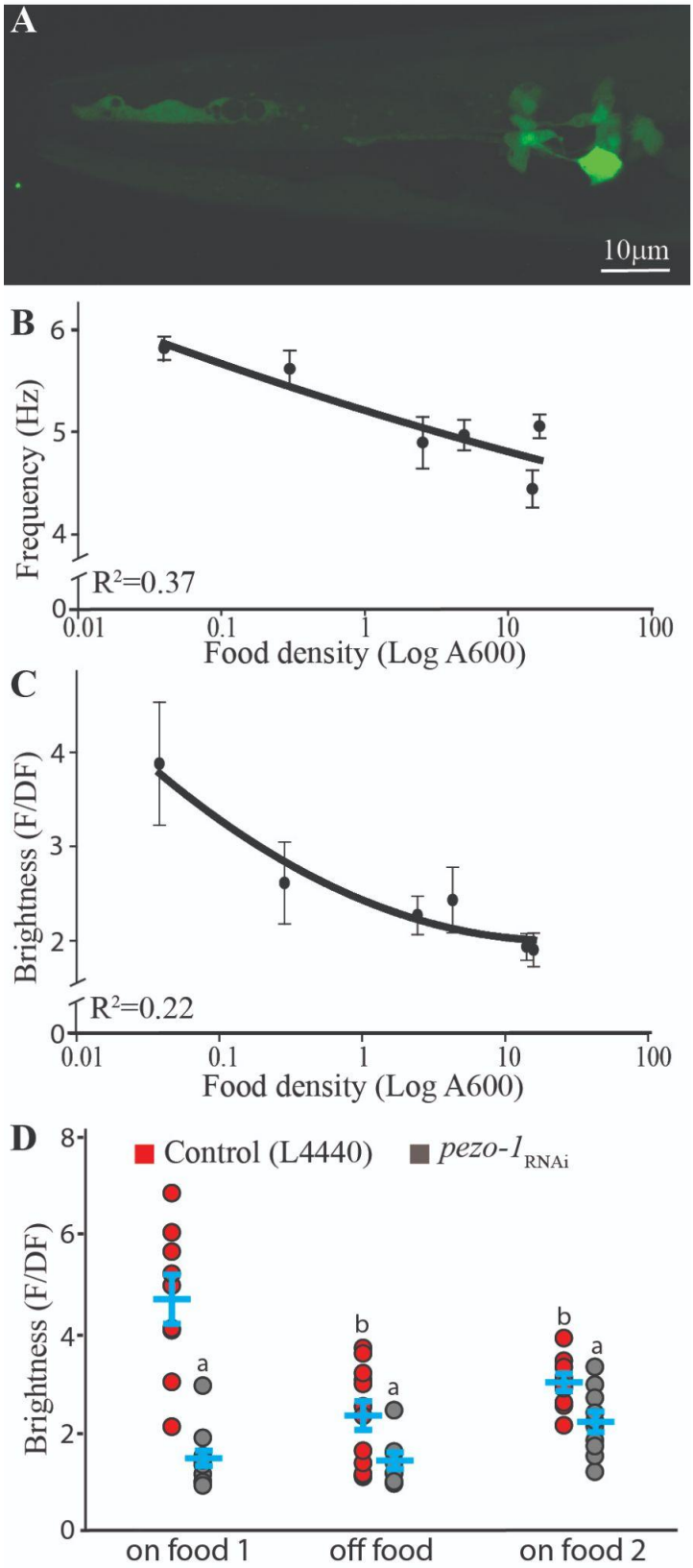


**Figure 6.**

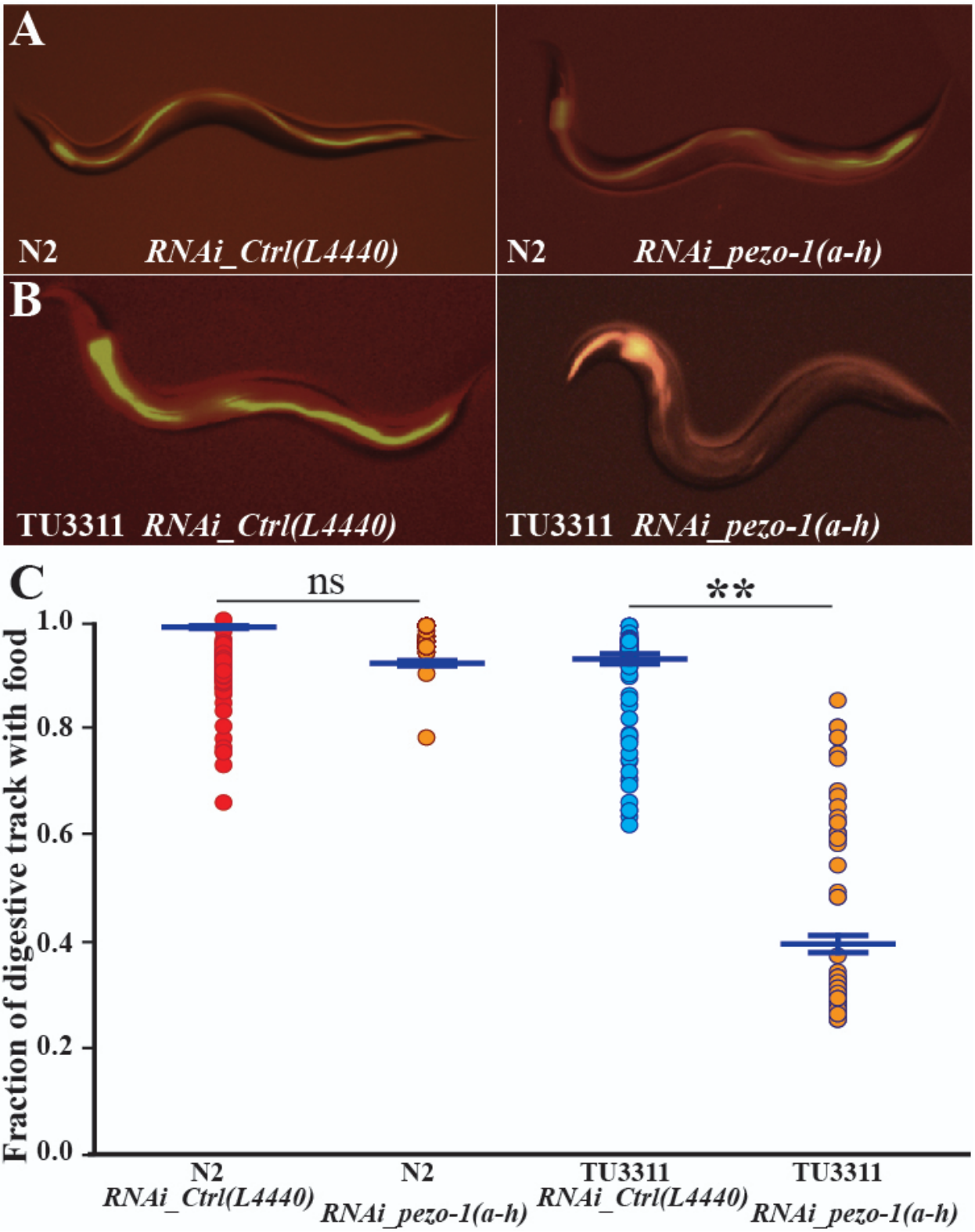


**Figure 7.**

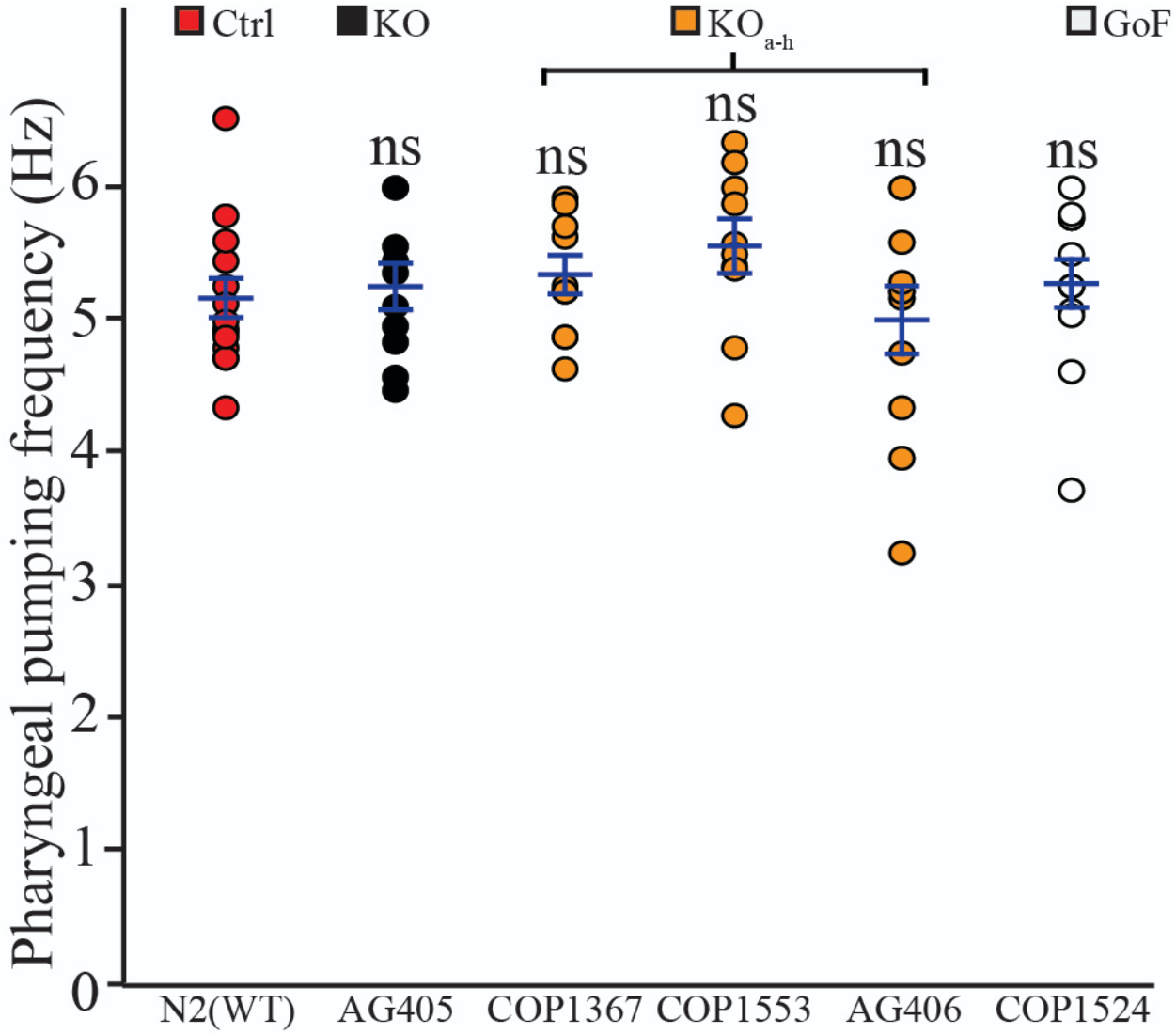


**Figure Supplementary 1.**

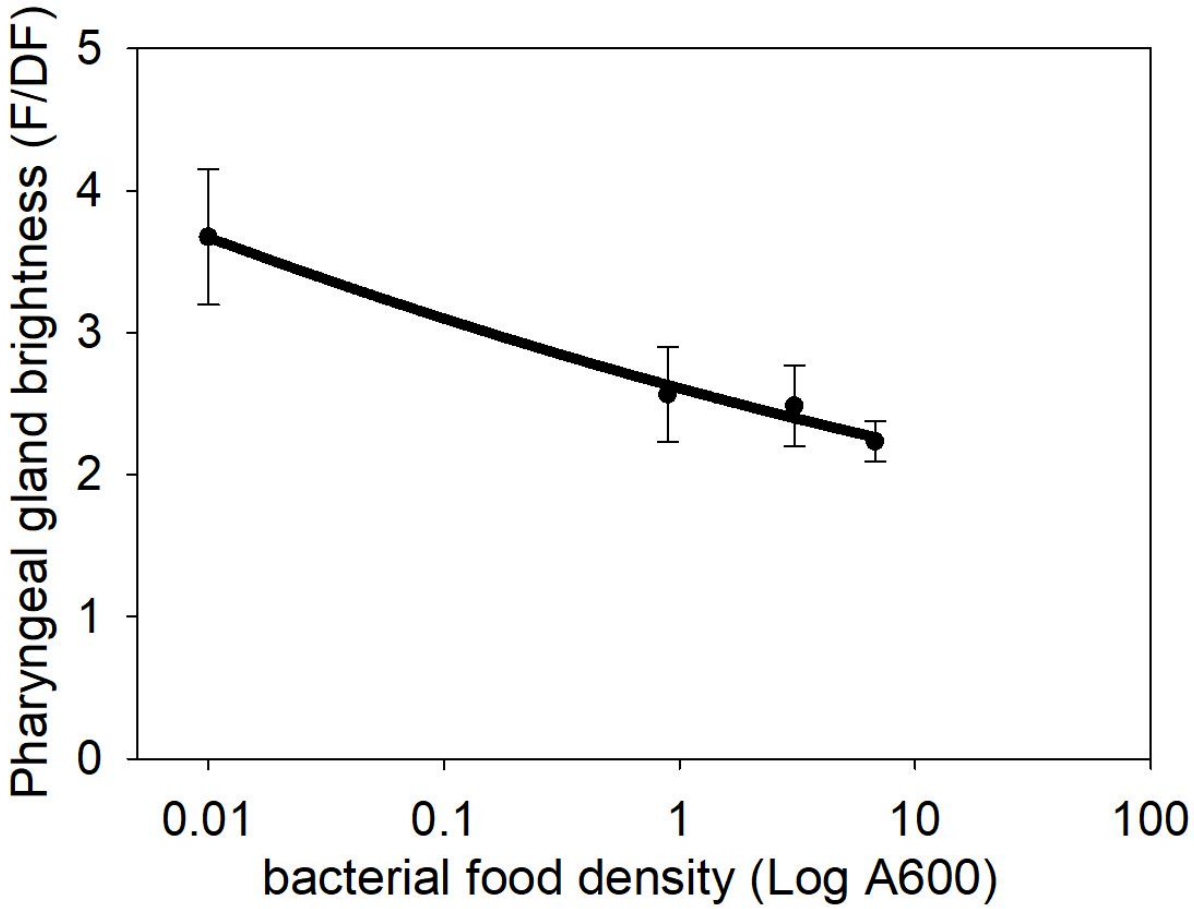


**Figure Supplementary 2.**